4B2-3

Effects of Soil Condition on Landmine Discrimination Using GPR Sensor

#Masahiko Nishimoto, Yusuke Kimura, and Takaaki Tanaka
Graduate School of Science and Technology, Kumamoto University
2-39-1 Kurokami, Kumamoto 860-8555, Japan, nisimoto@cs.kumamoto-u.ac.jp

1. Introduction

It is well known that a huge number of buried landmines in the post-war countries are still active, and that many civilians are killed or injured by landmine related accidents every year. Therefore, detection and clearance of buried landmines is a very important issue. Metal detectors are the almost universally available fielded devices for landmine detection, but they have great difficulty in detecting landmines that are made of plastic or with low metal content. On the other hand, Ground Penetrating Radar (GPR) is an emerging technique for landmine detection that can detect plastic or low metal content landmines. However, the GPR performs inadequately due to the ground clutter, because return from the shallowly buried landmine and that from ground surface overlap in time. Furthermore, the GPR also receives returns from other subsurface objects such as rocks, tree roots, or metal fragments in the ground, which yields high levels of false alarms. Generally speaking, the procedure for locating buried landmines using the GPR is divided into two stages, detection and identification. During the detection stage, all buried objects, including the desired landmines together with other objects such as stones, metal fragments, etc., are detected and their locations are specified. In the identification stage, the detected objects are classified and the landmines are differentiated from the other objects. The detection stage requires signal-processing techniques for radar target detection, whereas the identification stage requires pattern classification techniques. Compare with the detection process, the identification process is usually more complicated because considerable target information needs to be deduced from the total GPR data for reliable and accurate identification. Therefore, although many techniques for landmine detection when applied to GPR data have been proposed and designed to date, the development of reliable identification techniques is more important in reducing high incidence of false alarms. In this context, we here focus on the identification problem.

In the identification problem, selection of features used for target classification plays a key part because the classification performance depends strongly upon these features chosen. Therefore, in this research, we propose some kinds of features for landmine discrimination and evaluate the effects of soil condition on the performance through Monte Carlo simulations using a dataset generated by a 2-Dimensional Finite Difference Time Domain (2D-FDTD) method.

2. Features for Landmine Discrimination

Since we consider here the identification stage, we assume that the location of the buried object is already specified in the detection stage. Figure 1 shows the GPR system considered in this study. The measurements are conducted at M observation points above an uneven ground surface using a transmitting and receiving antenna pair. The transmitting antenna sends out a short duration pulse and the receiving antenna samples the returned signal that includes target response together with reflection from the rough ground surface. After removing the ground surface reflection [1][2] and enhance the target response [3], we extract the features for discriminating between potential landmine and clutter objects using a template of desired landmine. Figure 2(a) shows a landmine model considered in this study. This is the model of a Type-72 anti-personnel landmine, one of the most widely deployed landmines in Afghanistan. Since this bun-shaped landmine with a diameter of 7.8 cm and height of 4.0 cm has a small air gaps in a plastic casing, a response waveform for a

monocycle incident pulse has three peeks as shown in Fig. 2(b). Thus, we define the following four kinds of features:

(I) Normalized correlation (matched filter)

We define a normalized cross-correlation as a measure of waveform similarity using the following equation,

$$\overline{C}^{\max} = \max_{t} \frac{1}{\|\overline{x}\|\|\overline{s}\|} \int \overline{s}(\tau - t)\overline{x}(\tau)d\tau \qquad (1)$$

where $\overline{x}(t)$ and $\overline{s}(t)$ are the extracted target signal and reference template of the response from the landmine, respectively. Note that this normalized correlation $\overline{C}^{\max}$ becomes close to unity when $\overline{x}(t)$ has a similar part with $\overline{s}(t)$. Therefore, if the target signal $\overline{x}(t)$ includes the landmine response $\overline{s}(t)$, then the maximum correlation becomes close to unity at $t_m^{\max}$ that corresponds to the signal arrival time.

(II) Dispersion of signal arrival time

Since deviation of signal arrival times $t_m^{\max}$ measured at M observation points becomes close to the reference signal arrival time $t_m^{t\,\mathrm{arg}}$ obtained from the template when the signal $\overline{x}(t)$ includes the landmine response $\overline{s}(t)$, we can expect that variance of $t_m^{\max} - t_m^{t\,\mathrm{arg}}$ are one of the good features for landmine discrimination (see Fig. 3). Therefore, we define the following value as a feature.

$$V_T = \sum_{m=1}^{M} (t_m^{\max} - t_m^{t\,\mathrm{arg}})^2 \qquad (2)$$

(III) Time intervals between three peaks [3]

Since time intervals between three peaks of the response closely related to the structure of the object, we can expect that the time intervals are available as the features for landmine discrimination. Thus, we define the following time intervals T_{12} and T_{13} between these three peaks:

$$T_{12} = t_2 - t_1, \qquad T_{13} = t_3 - t_1 \qquad (3)$$

where t_1, t_2, and t_3 are the times when the peaks (1), (2), and (3) appear, respectively.

(IV) Amplitude ratios of three peaks

Amplitude ratios of these three peaks R_{12} and R_{13} defined by the following equations can also be available for the features for landmine discrimination,

$$R_{12} = -r_2 / r_1, \qquad R_{13} = -r_3 / r_1, \qquad (4)$$

where $r_1 = \overline{x}(t_1)$, $r_2 = \overline{x}(t_2)$, and $r_3 = \overline{x}(t_3)$. Schematic of these features are shown in Fig. 4.

3. Performance Evaluation

The discrimination performance is evaluated through Monte Carlo simulations. The 2D-FDTD method with PML absorbing boundary condition is employed for data generation. The landmine model and confusing objects are shown in Table 1. These objects are composed of homogeneous lossless dielectric. The depths of the landmine and confusing objects are varied between 2.0cm and 6.0cm. Each sample has a different surface roughness with Gaussian distributed height and slope. The monocycle input pulse is excited by Gaussian current, which parameters are chosen such that the incident field has most of its energy in the frequency band between 0.5GHz and 5GHz. Figure 5 shows one of the realizations of the surface roughness used for the numerical simulations. Roughness parameters (root mean square height h and correlation length l_c) are $h = l_c = 10$ mm. In order to estimate the effect of soil condition (surface roughness, soil inhomogeneity, and soil moisture), the discrimination performance is checked using ROC (receiver operating characteristic) curves and associated AUC (area under curve) values. However, we here show only the AUC values because of a page limitation. Table 2 shows AUC values for three different kinds of

surface roughness. This result indicates that the best feature for discriminating between landmines and confusing objects is $\overline{C}^{\,\max}$ and AUC value of about 99% is achieved for rough case. Table 3 and 4 show AUC values for check the effects of soil inhomogeneity and soil moisture, respectively. These results indicate that the correlation $\overline{C}^{\,\max}$ is the best and time interval T_{12} is a comparatively good feature for landmine discrimination when the soil condition is changed.

4. Conclusions

We have introduced some kinds of features for landmine discrimination and evaluate the effects of soil condition on the discrimination performance through Monte Carlo simulations. We have confirmed from the simulation results that sufficient discrimination performance could be obtained when the soil condition is changed. We can expect that a feature vector constructed by a combination of $\overline{C}^{\,\max}$ and T_{12} would give more satisfactory performance.

References

[1] H. Brunzell, "Detection of shallowly buried objects using impulse radar," *IEEE Trans. Geosci. Remote Sens.,* vol. 27, no. 2, pp. 875-886, 1999.

[2] C. Rappaport, *et al*., "Suppressing GPR clutter from randomly rough ground surfaces to enhance nonmetallic mine detection," *Subsurface Sensing Tech. and Applicat.*, vol. 4, no.4, 2003.

[3] M. Nishimoto *et al.*, "Classification of landmine-like objects buried under rough ground surfaces using a ground penetrating radar," *IEICE Trans. Electron.*, vol. E90-C, no. 2, pp. 327-333, 2007.
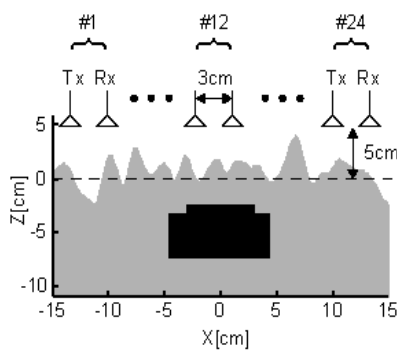
Figure1: GPR system for landmine discrimination.
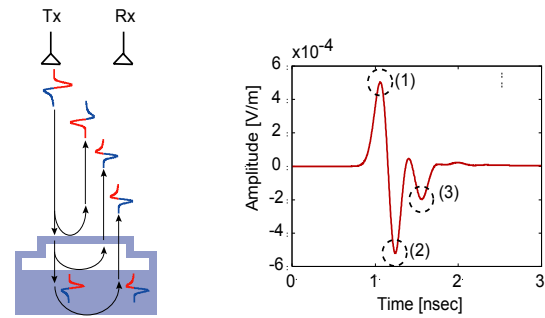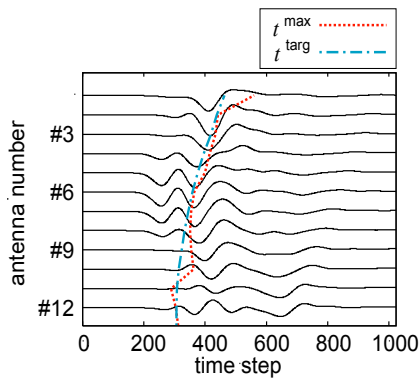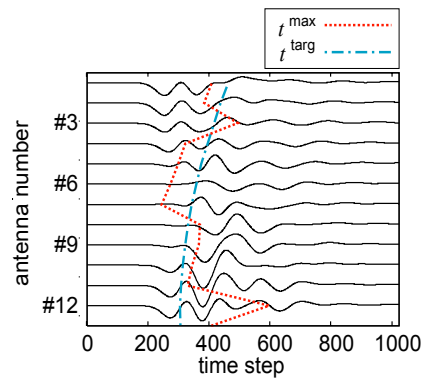

(a) Return paths   (b) Return signal

Figure2: Landmine model and return signal.

(a) Landmine model

(b) Confusing object
(randomly deformed circular cylinder)

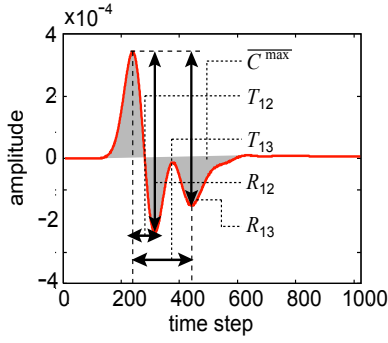Figure3: Comparison of the signal arrival time $t_m^{\max}$ and $t_m^{t\,\mathrm{arg}}$.
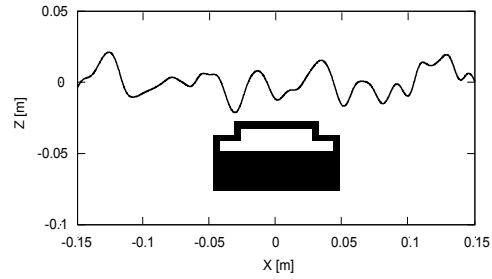
Figure 4: Schematic of the features.

Figure 5: One of the realizations of the rough ground surfaces used for the simulations.
($h = l_c = 10$ mm, $\varepsilon_r = 4.0$, $\sigma = 0.0842$ [S/m])

Table 1: Landmine model (target) and three kinds of confusing clutter objects.

Type	Shape	Size		ε_r	Depth d	Number of samples
Landmine model (target)		$W = 6.0$ cm (top), 9.0 cm (bottom) $H = 5.0$ cm $= 1.0$ cm (top) + 4.0 cm (bottom) Width of the air gap = 1.5 cm		3.0	2.0cm	300
Confusing clutter objects		(a)	Randomly deformed elliptic cylinders $W = 9.0 \pm 0.5$ cm , $H = 5.0 \pm 0.5$ cm	3.0	3.0cm 4.0cm	100
		(b)	Randomly deformed circular cylinders $D = 5.0 \pm 0.5$ cm		5.0cm 6.0cm	100
		(c)	Randomly deformed slabs $W = 9.0 \pm 0.25$ cm , $H = 2.2 \pm 0.25$ cm			100

Table 2: ROC-AUC values for three kinds of surface roughness
($h = l_c = 10$ mm, $\varepsilon_r = 4.0$, $\sigma = 0.0842$ [S/m])

Surface roughness	ROC-AUC values for the features [%]					
	$\overline{C}^{\max}$	V_T	T_{12}	T_{13}	R_{12}	R_{13}
$h = 10$ [mm], $l_c = 10$ [mm] (rough)	99.3	89.9	97.7	92.9	82.8	95.0
$h = 10$ [mm], $l_c = 20$ [mm]	99.1	82.6	95.8	91.0	78.0	94.4
$h = 10$ [mm], $l_c = 50$ [mm] (smooth)	99.1	91.3	97.4	94.8	72.9	97.8

Table 3: ROC-AUC values for inhomogeneous soil. ($h = 10$ mm, $l_c = 10$ mm)

Inhomogeneity of soil	ROC-AUC values for the features [%]					
	$\overline{C}^{\max}$	V_T	T_{12}	T_{13}	R_{12}	R_{13}
$\varepsilon_r = 4.0$ (homogeneous)	99.3	89.9	97.7	92.9	82.8	95.0
$\varepsilon_r = 5.5 \pm \Delta\varepsilon_r(x, z)$ (inhomogeneous)	96.6	82.2	86.1	79.1	75.8	89.5

Table 4: ROC-AUC values for soil moisture. ($h = 10$ mm, $l_c = 10$ mm)

Moisture of soil	ROC-AUC values for the features [%]					
	$\overline{C}^{\max}$	V_T	T_{12}	T_{13}	R_{12}	R_{13}
$\varepsilon_r = 4.0$, $\sigma = 0.0824$ [S/m] (dry)	99.3	89.9	97.7	92.9	82.8	95.0
$\varepsilon_r = 8.0$, $\sigma = 0.253$ [S/m] (medium)	83.2	70.4	75.1	77.3	62.1	51.7